Progress In Electromagnetics Research C, Vol. 117, 17–30, 2021

Staired-Slitted Flag Central Resonator Based Wide Band Bandpass Filter for Super Spurious Harmonic Suppressions

Ami Iqubal* **and Parambil Abdulla**

Abstract—A novel staired-slitted flag central resonator based wide band bandpass filter with sharp selectivity and super spurious harmonic suppression is proposed in this paper. Input-output ports based on three line edge coupling with ground plane aperture cutting contribute to the rejection of harmonics in the lower stopband. The spurious harmonic at the upper stopband is rejected with the help of embedded open stub suppression cells. The generation of two transmission zeros at the lower and upper cut-off frequencies are due to the staired slitted-flag main resonator, which contributes to the better selectivity of the filter, and it is verified with the help of mathematical equations. The fractional bandwidth of the developed filter is 107.2% with 7.82 GHz centre frequency. This work demonstrates the design, theory, and implementation aspects for the realization of bandpass filters with sharp selectivity and very good spurious suppression.

1. INTRODUCTION

The demand for bandpass filters with characteristics such as wide passband, sharp roll off rate, and super spurious suppressions capability is increasing day by day as they are the key elements in microwave wideband communication systems. Varieties of bandpass filter design techniques have been proposed over the past decades for the realization of filters with desired features. In [1], wideband filter configuration with a triple mode resonator is reported. But it lacks wideband spurious suppression capability. A filter based on extended tapped lines with high selectivity is investigated in [2], but the stopband suppression achieved is only 14.5 dB. An ultra-wideband (UWB) filter by cascading two miniaturized low pass and high pass modules is discussed in [3]. Even though the fractional bandwidth is high, the out of band performance is poor. A filter design using T-shaped transmission lines and coupled lines is discussed in [4], but the sharpness factor of the filter needs space for improvement. A wide stopband bandpass filter design employing uniform impedance resonators with via is demonstrated in [5]. However, this structure suffers from narrow passband. In [6], a bandpass filter with ultra-wide passband and sharp roll off based ona CPW to microstrip coupling structure is implemented. Despite these features, this structure suffers from poor return loss performance of the passband. The filter design demonstrated in [7–11] suffers from sharp selectivity. The design of filters depicted in [12–18] involves complex methods which require sophisticated procedures for achieving the narrow spacing between adjacent lines. For improving the selectivity of the structure, various methods are discussed in [19–25]. Techniques for improving the stopband suppression are analyzed in [26, 27]. The fractional bandwidths of the filters in [28–31] are low. The outcome obtained from the aforementioned review is that there is still need for simple filter design methods that enable the easy realization of wideband filters with very low passband insertion loss, wide passband with very good selectivity, very good return loss in the passband, and spurious free stopbands.

Received 30 September 2021, Accepted 1 December 2021, Scheduled 9 December 2021
* Corresponding author: Ami Iqubal (amiiqubal@cusat.ac.in).
The authors are with the Division of Electronics, School of Engineering, CUSAT, Cochin, Kerala 22, India.

This work demonstrates the implementation of a bandpass filter with a staired-slitted flag central resonator, embedded open stubs, and rectangular aperture slit based three line edge coupled lines. Spurious harmonic suppression at the higher cut-off frequencies is achieved by the four embedded open stub loaded resonators. Meanwhile, for achieving the lower spurious skirt rejection, input-output feed lines with three line edge coupling is employed. This structure can ensure ultra-wide passband, super spurious rejections, and very good roll-off rate. The proposed filter is simulated, fabricated, and measured. The measured results are at par with simulated predictions.

2. DESIGN AND ANALYSIS OF THE FILTER STRUCTURE

The proposed filter structure with three-dimensional configuration and dimensions are shown in Figures 1(a) and 1(b), respectively. The substrate used for the prototype development was RT/Duroid 5880. Substrate thickness of the material, $t = 0.79\,\text{mm}$, loss tangent = 0.0009, and $\varepsilon_r = 2.2$. The top layer consists of a central resonator and embedded open stubs coupled with input output feed lines. Two rectangular slots are etched in the bottom layer as shown in Figure 1(b). Design of the proposed filter is carried out as detailed below.

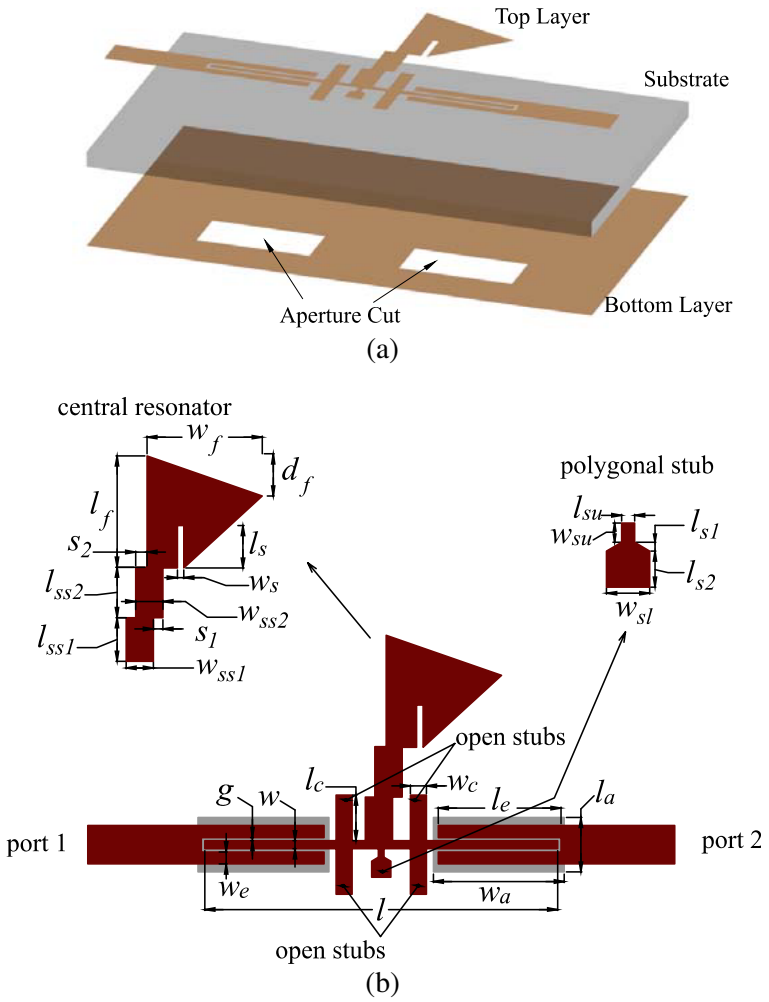

Figure 1. (a) 3D view of the filter. (b) Layout of the proposed structure with dimensions.

2.1. The Design of Staired-Slitted Flag Central Resonator

The sharp transition from passband to stopband is one of the essential prerequisites that have to be ensured while bandpass filters are designed. For achieving this, the allocation of attenuation poles near the transition band edges is a must. In this work, a compact staired-slitted flag central resonator (SFR) consisting of two high-low impedance regions is employed for the generation of attenuation poles.

The layout and LC equivalent circuit developed for SFR are depicted in Figures 2(a) and (b) respectively with the inductive and capacitive parameters as $L_a = 3.414\,\text{nH}$, $C_a = 0.0548\,\text{pF}$, $L_b = 4.1527\,\text{nH}$, and $C_b = 0.6368\,\text{pF}$. The elemental values $L_{p1} = L_{p2} = 1\,\text{nH}$ and $C_{g1} = C_{g2} = 0.25\,\text{pF}$ contribute to impedance matching. The physical dimensions of the SFR are depicted in Table 1. MATLAB program for finding out transmission characteristics of the SFR is developed with respect to Figure 2(b) having the overall characteristic impedances Z_A, Z_B, and Z_C respectively as given in Equations (1)–(3).

$$Z_A = SL_{p1} \tag{1}$$

$$Z_C = SL_{p2} \tag{2}$$

$$Z_B = \frac{\left[C_{g1}C_{g2}(S^2C_aC_b(L_a+L_b)+C_a+C_b)\right]+L_{p1}(C_{g1}+C_{g2})\left[S^4L_aL_bC_aC_b+S^2L_aC_a+S^2L_bC_b+1\right]}{S^2C_{g1}\left[S^2C_aC_b(L_a+L_b)+(C_a+C_b)\right]} \tag{3}$$

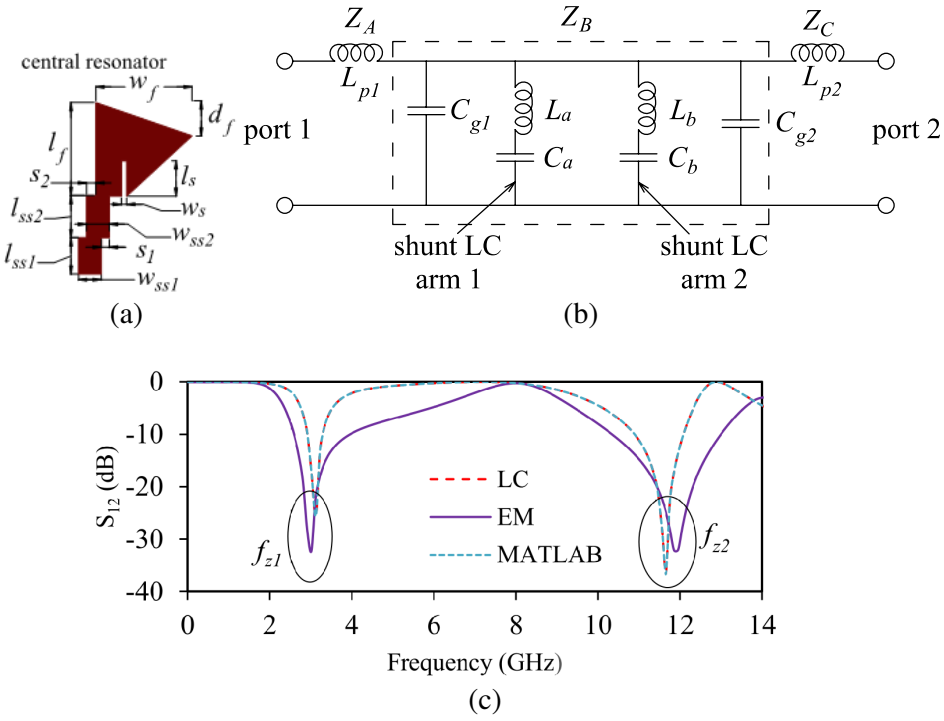

Figure 2. (a) Layout of the central SFR with dimensions. (b) Equivalent circuit of the central resonator. (c) Comparison of transmission characteristics by EM, LC and MATLAB simulations.

Table 1. The physical dimensions of the SFR.

Parameter	Units	Parameter	Units	Parameter	Units
l_{ss1}	2.7 mm	w_s	0.4 mm	w_{ss1}	1.70 mm
l_{ss2}	3.2 mm	l_f	7 mm	l_s	2.65 mm
s_1	0.6 mm	w_f	6 mm	w_{ss2}	1.70 mm
s_2	0.6 mm	d_f	2 mm	t	0.79 mm

The approach used here is the derivation of ABCD parameters from the equivalent characteristic impedances and thus obtaining the scattering parameters. The transmission characteristics of the SFR are plotted using IE3D simulation software (EM), by equivalent circuit (LC) method and with MATLAB programs thereby locating the positions of transmission zeros (f_{z1} and f_{z2}) at 3.1 GHz and 11.65 GHz as shown in Figure 2(c). The slight change in attenuation pole locations is because when equivalent circuit model is developed, substrate loss tangent could not be considered.

The contributing elements for the lower and upper transmission zeros are obtained through parametric analysis of L_a, C_a and L_b, C_b as depicted in Figures 3(a) and 3(b), respectively. The considered variations of capacitance C_a are from 0 pF to 0.1 pF, and C_b is from 0 pF to 4 pF. The range of L_a and L_b analyzed is from 0 nH to 8 nH. In Figure 3(a), C_a vs. f_{z1} and C_a vs. f_{z2} denote the variations of lower transmission zero (f_{z1}) and upper transmission zero (f_{z2}) with respect to C_a. Similarly, L_a vs. f_{z1} and L_a vs. f_{z2} denote the variation of lower transmission zero (f_{z1}) and upper transmission zero (f_{z2}) with respect to L_a. From Figure 3(a), it is clear that L_a and C_a variation affects the location of f_{z2}, and thus we can assert that shunt LC arm 1 controls upper transmission zero.

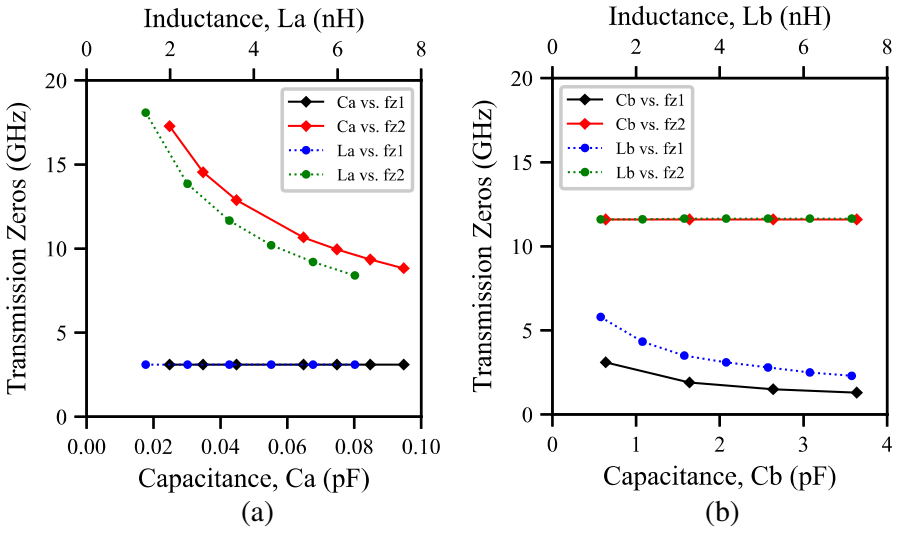

Figure 3. Parametric analysis of (a) shunt LC arm 1, (b) shunt LC arm 2 with respect to transmission zero locations.

In Figure 3(b), C_b vs. f_{z1} and C_b vs. f_{z2} denote the variations of lower transmission zero (f_{z1}) and upper transmission zero (f_{z2}) with respect to C_b. Similarly, L_b vs. f_{z1} and L_b vs. f_{z2} denote the variations of lower transmission zero (f_{z1}) and upper transmission zero (f_{z2}) with respect to L_b. Figure 3(b) shows that shunt LC arm 2 (L_b and C_b) controls the location of lower transmission zero. For our design, in order to fix the location of f_{z1} and f_{z2}, the optimized values for $L_a = 3.414$ nH, $C_a = 0.0548$ pF, $L_b = 4.1527$ nH, and $C_b = 0.6368$ pF are selected. Out of band spurious responses can be suppressed as explained in the following sections.

2.2. The Higher Harmonic Suppression Using Embedded Open Stubs

To the SFR, four open stub cells with dimensions $l_c = 2.85$ mm and $w_c = 1$ mm are embedded for creating transmission zeros at upper stopband, as these stubs can create band gap effect. This generates a transmission zero at 17.6 GHz, thereby the cascaded SFR-open stub can reject higher harmonics up to 20 GHz as depicted in Figure 4. From this graph, it is clear that the transmission zero generated by the four open stubs help to suppress the upper stopband spuriousity of the SFR. Even though the higher harmonic suppression is achieved, the lower stopband performance needs room for improvement. Lower spurious suppression can be achieved as detailed in Section 2.3.

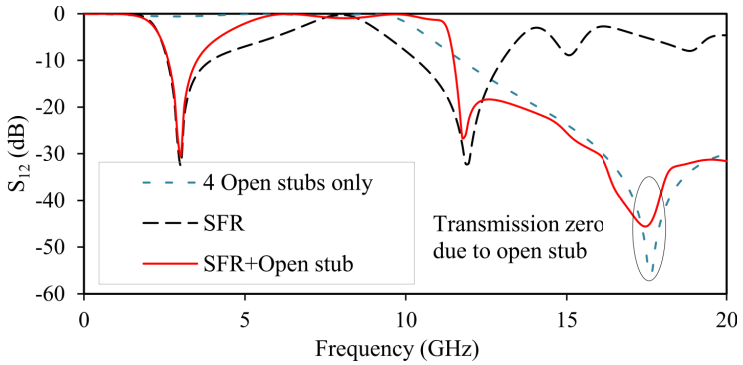

Figure 4. Comparison of transmission characteristics of SFR only, 4 open stubs only and SFR + open stubs together.

2.3. Ground Plane Aperture (GPA) Based Input-Output Coupling for Lower Harmonic Suppression

Three line input output (I/O) coupled lines with slotted ground plane aperture are applied to the open stub loaded SFR for reducing lower stopband spuriousity. The dimensions are mentioned in Table 2. An aperture slit is made in the ground plane exactly behind the edge coupled lines for ensuring tight coupling without compromising minimum gap achievable between two lines using normal fabrication procedures. The three lines having tight edge coupling provide two attenuation poles at locations 0 GHz and at 14.2 GHz by offering suppressions of −60 dB and −35 dB, respectively.

Table 2. The physical dimensions of the GPA loaded I/O coupled lines.

Parameter	Units
w_e	0.80 mm
l_e	7.75 mm
g	0.20 mm
l_a	3.40 mm
w_a	8.17 mm
w	0.50 mm
l	22.00 mm

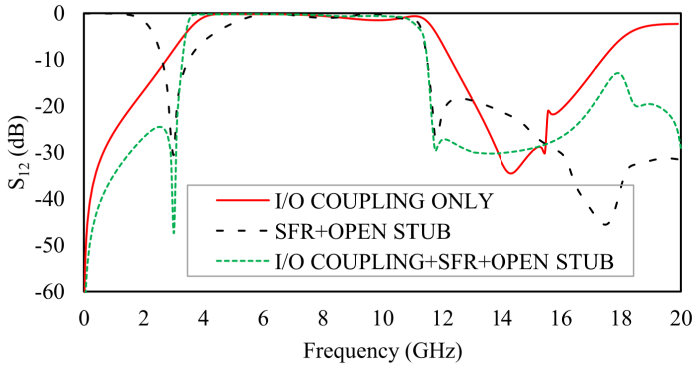

Figure 5. Comparison visualization of lower harmonic suppression by double stage line edge lines with ground plane aperture coupling.

The role of I/O coupling in suppressing lower harmonics is demonstrated in Figure 5. This graph depicts the transmission characteristics comparison of staired-slitted flag central resonator and open stub (in dotted black colour), input-output three-line edge coupled lines (red colour), and their combined effect (in green colour). The cascading of edge coupled lines to the four open stub loaded SFR shifts the attenuation zero with 0 dB to −60 dB suppression level. At 17.9 GHz, the combined filter response shows a spike of attenuation pole with −13.88 dB rejection level. For improving the overall filter response, polygonal stubs are introduced as discussed in the next section.

2.4. Design of Stepped Polygonal Stub Cells for Wideband Harmonic Suppression

Even though the cascading of I/O coupled lines achieved spurious harmonic suppression at lower stopband, it shifts the rejection level of upper outband transmission zero (f_z) to −13.88 dB suppression level. For improving the higher harmonic rejection capability, a stepped polygonal stub cell with the structural values as shown in Table 3 is introduced. It generates a transmission zero at 22.08 GHz thereby rejecting the harmonics at higher frequencies. Layout and equivalent circuit for this structure

Table 3. Geometrical parameters of the proposed stepped polygonal stub cell.

Parameter	Units
l_{su}	0.36 mm
l_{s1}	0.25 mm
w_{sl}	1.20 mm
w_{su}	0.53 mm
l_{s2}	1.00 mm

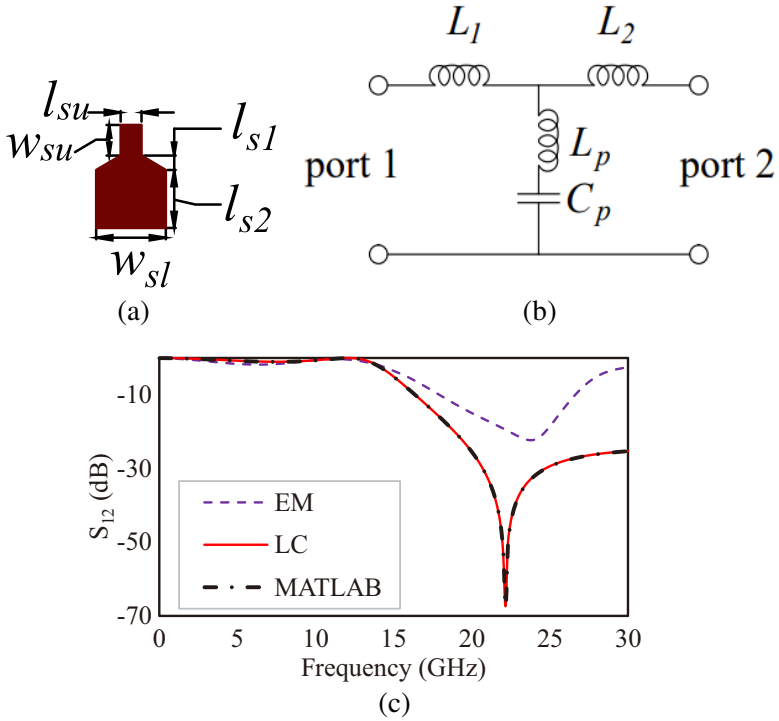

Figure 6. (a) Layout of the stepped polygonal stub with dimensions. (b) Equivalent circuit of the stepped polygonal stub. (c) Comparison of transmission characteristics by EM, LC and MATLAB simulations.

with values $L_1 = L_2 = 1\,\text{nH}$, $L_p = 0.304\,\text{nH}$, and $C_p = 0.17\,\text{pF}$ are as shown in Figures 6(a) and (b), respectively. MATLAB coding is done for verifying the correctness of the developed equivalent circuit. The comparison of transmission characteristics in LC, EM, and MATLAB methods is done as depicted in Figure 6(c), and it verifies the correctness of equivalent circuit.

By the introduction of the stepped polygonal stub, the overall filter response got improved as demonstrated in Figure 7. The solid line (red colour) shows the transmission characteristics after adding lower stepped polygonal stub which shows spurious free response up to 20 GHz.

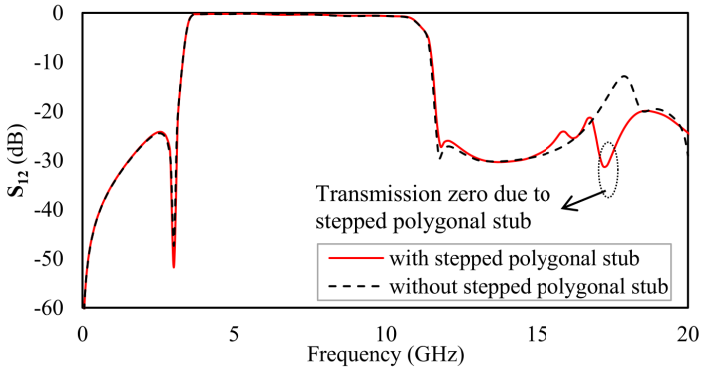

Figure 7. Comparison of overall transmission characteristics with and without stepped polygonal stub.

The dotted line (black colour) depicts the spuriousity at 17.9 GHz when there is no lower stepped polygonal stub. The low pass filter characteristics of the stepped polygonal stub are utilized for improving overall filter performance here.

3. DESIGN EVOLUTION AND RESONANCE ANALYSIS OF THE PROPOSED FILTER STRUCTURE

The structural evolution and the IE3D software simulated transmission and reflection responses of the proposed filter are depicted in Figure 8. The passband attenuation zero obtained from the SFR is illustrated in Figure 8(a), which is located at 8.04 GHz with −24.74 dB suppression level. The loading of four open stubs to the SFR improves the insertion loss by providing better coupling. The transmission poles in the passband of the open stub loaded SFR are located at 6.33 GHz, 9.74 GHz, and 11.05 GHz with suppression levels −43.82 dB, −21.56 dB, and −7.8 dB, respectively as depicted in Figure 8(b). The open stub loaded SFR as shown in Figure 8(b) has one attenuation zero at 0 GHz with −52 dB suppression level which causes the unwanted spuriousity at lower stopband. In Figure 8(c), GPA based I/O coupling nullifies the transmission pole at 0 GHz thereby ensures out of band spurious suppression at lower stopband. The attenuation zeros or resonant modes as presented in Figure 8(c) at passband locations 3.72 GHz, 4.32 GHz, 5.32 GHz, 7.73 GHz, 9.54 GHz, and 10.55 GHz with suppression levels −26.36 dB, −28.68 dB, −36.8 dB, −41.26 dB, −21.45 dB, and −15 dB enhance the strong coupling and thereby improve the passband performance. Figure 8(d) depicts the improved characteristics of the filter after the addition of stepped polygonal stub for higher harmonic spurious suppressions.

4. PARAMETRIC ANALYSIS

The role of each parametric element in the transmission and reflection performance of the filter is presented in this section.

4.1. Parametric Analysis of Slit Length and Width of the SFR

The importance of the length and width of the slit in the SFR is analyzed as shown in Figure 9. For improving the passband characteristics of the filter, a slit is introduced to the SFR, and parametric

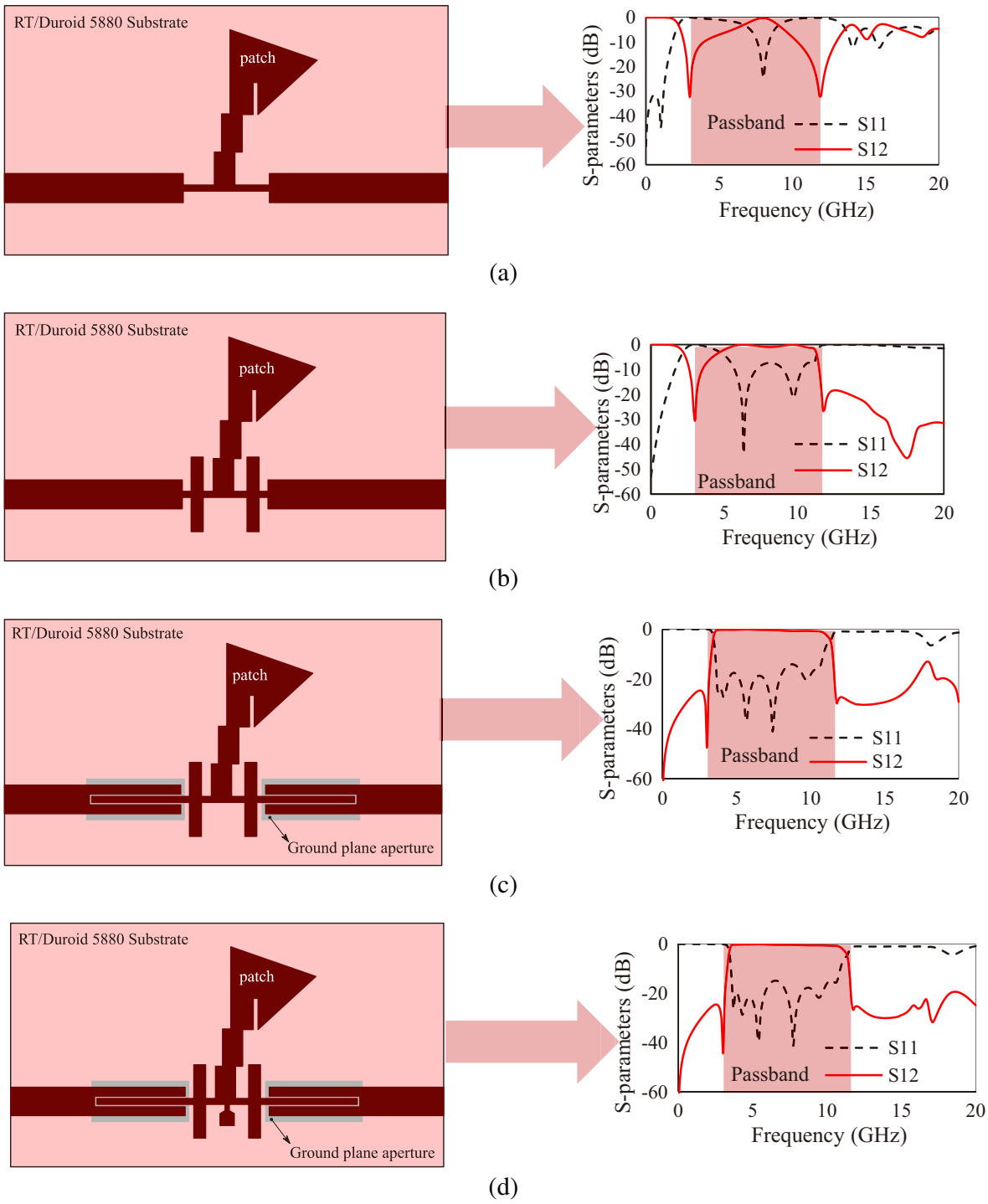

Figure 8. Structural evolution and improvements in the characteristics of the proposed filter (a) SFR only, (b) embedded open stub loaded SFR, (c) ground plane aperture based embedded open stub loaded SFR, (d) polygonal stub loaded ground plane aperture based embedded open stub loaded SFR.

analysis is carried out for finalizing the length and width of the slit. Slit length and width are varied from 0 mm to 4.65 mm and 0 mm to 0.8 mm, respectively. Figures 9(a) and (b) respectively depict that when there is no slit in the central resonator, the passband to stopband performance of the filter is poor. As the length and width of the slit are varied, the transmission characteristics show significant changes

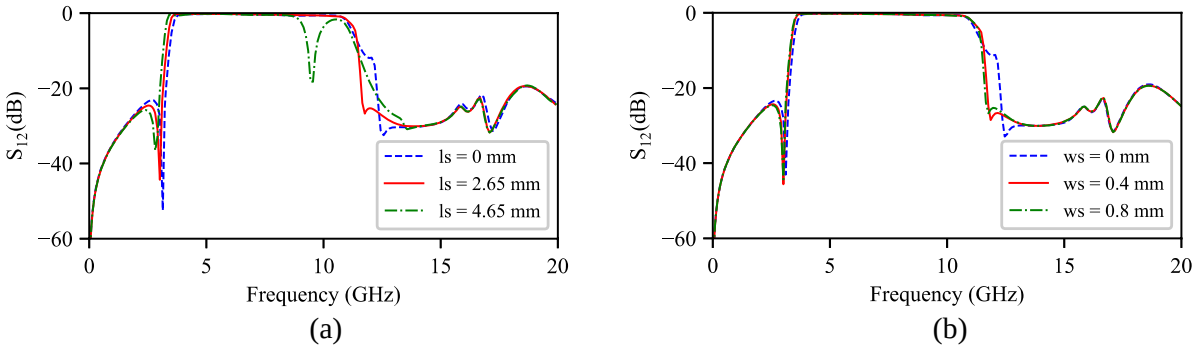

Figure 9. Parametric analysis of (a) slit length, (b) slit width with respect to transmission characteristics.

in the upper stopband transition. The introduction of a slit with $l_s = 2.65\,\text{mm}$ and $w_s = 0.4\,\text{mm}$ makes the filter performance superior with smooth upper passband to stopband transition.

4.2. Parametric Analysis of Ground Plane Aperture Width

An aperture slit is made in the ground plane exactly behind the three line edge coupling for ensuring tight coupling without compromising minimum gap achievable between two lines using normal fabrication procedures. For optimising the width of the aperture cut, parametric analysis is carried out for width

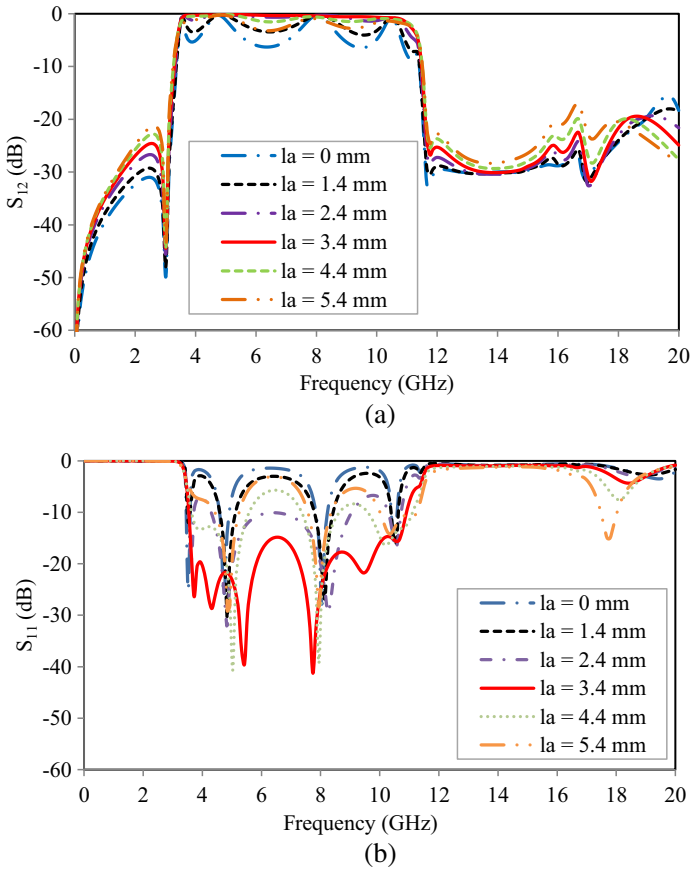

Figure 10. Parametric study of ground plane aperture width, (a) transmission characteristics, (b) reflection characteristics.

of the aperture, l_a, from 0 mm to 5.4 mm as shown in Figures 10(a) and (b). When $l_a = 0$ mm, the passband of the filter shows ripples with very high insertion loss. This happens because when there is no slit, the coupling is very small. As l_a is increased, the coupling is improved, and for $l_a = 3.4$ mm, we get optimum performance. The reflection characteristics also show better performance for $l_a = 3.4$ mm. When $l_a = 0$ mm, due to very poor coupling effect, the passband return loss shows poor performance. As l_a is further increased beyond 3.4 mm, the upper out of band performance shows spuriousity beyond 18 GHz, and thus the ideal value for ground plane aperture width is selected as 3.4 mm.

4.3. Ground Plane Aperture Length Parametric Study

For optimising the aperture cut length, parametric analysis is carried out for length of the aperture, w_a from 0 mm to 12.17 mm as shown in Figure 11. When $w_a = 0$ mm, the passband of the filter exhibits ripples with very high insertion loss. This happens because when there is no slit, the coupling is very weak. Parametric study is carried out for 0 mm to 12.17 mm. As w_a is increased, the coupling is improved and for $w_a = 8.17$ mm, we get optimum performance. The reflection characteristics also shows best performance for the chosen $w_a = 8.17$ mm. As w_a is further increased beyond 8.17 mm, the upper out of band performance shows spuriousity around 16 GHz and thus the ideal value for ground plane aperture length is selected as 8.17 mm.

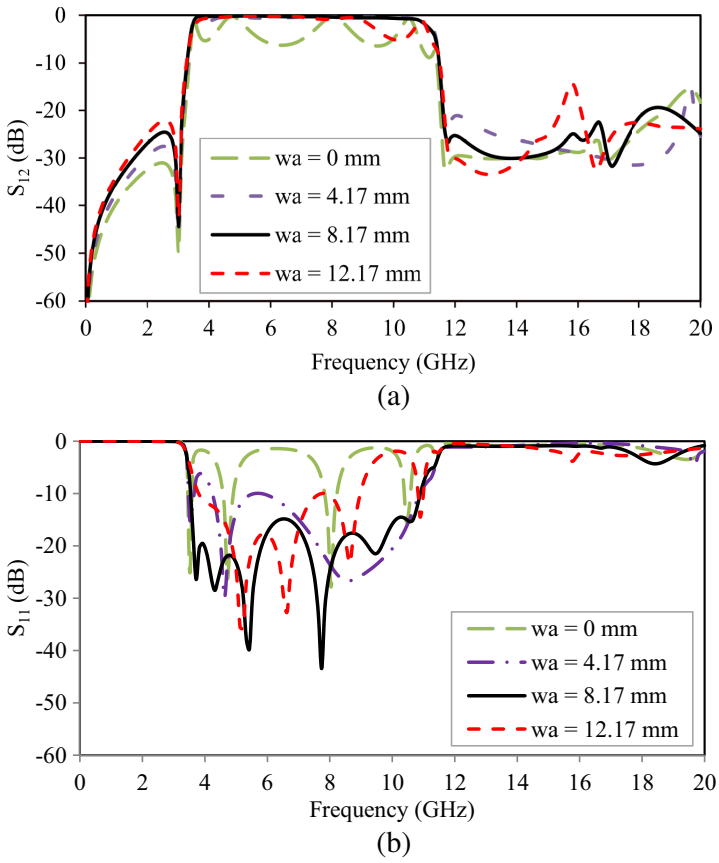

Figure 11. Parametric study of ground plane aperture length, (a) transmission characteristics, (b) reflection characteristics.

5. RESULTS AND DISCUSSIONS

The simulation and optimization of the filter structure are carried out using IE3D and fabricated using photolithographic procedures on an RT/Duroid 5880 substrate, with a loss tangent = 0.0009 and $\varepsilon_r = 2.2$. The measurements are obtained using Agilent N5227A network analyzer.

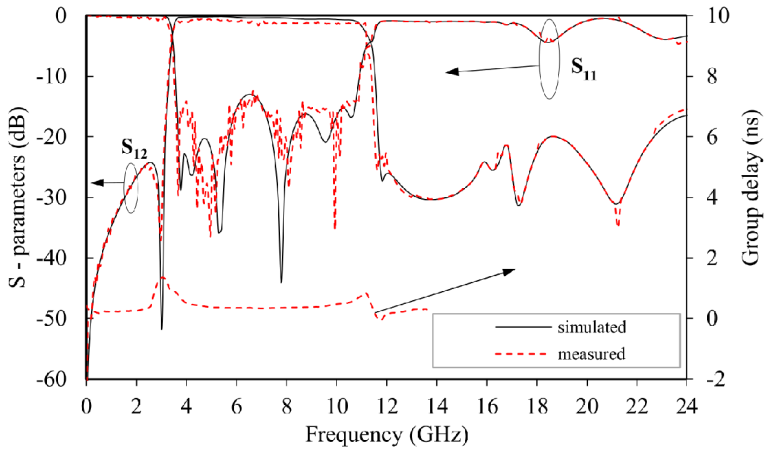

Figure 12. Measured and simulated response of the filter.

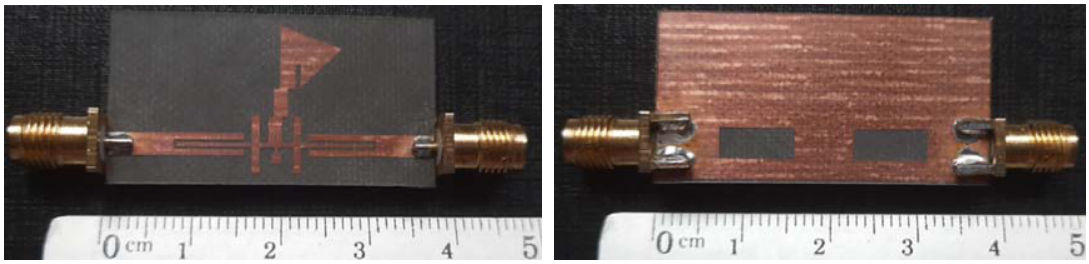

Figure 13. Photograph of the developed filter structure. (a) Top view. (b) Bottom view.

The simulated and measured results of the developed filter are shown in Figure 12, and photographs of the fabricated structure are given in Figure 13. The passband of the filter exhibits six attenuation zeros at frequency locations of 3.72 GHz, 4.32 GHz, 5.32 GHz, 7.73 GHz, 9.54 GHz, and 10.55 GHz. Wide passband of the filter is attributed by these attenuation zeros. Sharp selectivity is contributed by a stepped slitted flag central resonator which generates two transmission zeros at locations near the lower and upper cut-off frequencies 2.98 GHz and 11.63 GHz with suppression levels -37.2 dB and -25.8 dB, respectively. SFR is arranged in the form of a stair instead of straight stub for making the structure more compact, and the flag shaped tapering of the central resonator is introduced for ensuring better reflection characteristics. The lower spurious harmonic suppression achieved is better than -24.6 dB, and the higher harmonics can be rejected up to 22.65 GHz with -20 dB suppression level. Very good out of band spurious suppression performance of this filter is achieved by the combined action of embedded open stubs, stepped polygonal stubs, and ground plane aperture based input-output coupled lines. Four embedded open stubs and stepped polygonal stubs contribute towards the suppression of higher harmonic spuriousity. Lower harmonic spurious suppression capability of the filter is obtained by the ground plane aperture based input output coupled lines. The measured return loss is better than 14 dB, and the passband insertion loss is less than 0.4 dB.

The normalized circuit size of the developed filter is only $0.77\lambda_g \times 0.44\lambda_g$. Measured attenuation slopes corresponding to the lower and upper cut-off frequencies are 86.75 dB/GHz and 64.81 dB/GHz, respectively. A comparison of the developed filter with relevant existing works is depicted in Table 4, which underlines the merits of very good harmonic suppression and very good fractional bandwidth.

Table 4. Comparison of developed filter with existing works.

References /Parameters	Fractional bandwidth (%)	Harmonic suppression (GHz)	Insertion Loss @Centre Frequency (dB)	Rejection level (dB)	Centre frequency (GHz)	Dielectric constant, ε_r/thickness, t (mm)
[16]	40	16.7	0.7	> 20	5	3.4/0.508
[18]	59.25	16	2.2	-31.6	6.025	3.66/0.508
[19] Filter 1	64.83	4.76	0.63	-20	1.01	3.58/0.0027
[23] Filter 1	1.8	5.5	< 0.7	11	2.7	2.2/0.508
[24]	97.57	24.2	1.62	-20	5.68	4.4/0.8
[28]	77.5	19.94	0.65	< -20	1.69	3.66/0.508
[29]	39.8	7.69	0.65	< -15	2.33	2.2/0.508
[30]	20.5	1.48	0.65	-32	0.33	10.2/1.28
This work	**107.2**	**22.65**	**0.4**	$\mathbf{> -20}$	**7.82**	**2.2/0.79**

6. CONCLUSION

In this paper, the emergence of two transmission zeros at passband edges with the help of stepped-slitted flag central resonator is demonstrated. The achievement of spurious free stopband by using three line edge coupled feed lines and embedded open stubs is depicted with the help of detailed analysis. The effect of length and width of the SFR slit is studied in detail, and their significance in achieving sharp roll off of the filter is verified. The developed filter structure with very good passband and stopband characteristics having very simple design methodology makes this filter an ideal candidate for ultra wide band applications.

REFERENCES

1. Zhu, L., S. Sun, and W. Menzel, "Ultra-wideband (UWB) bandpass filters using multiple-mode resonator," *IEEE Microw. Wireless Compon. Lett.*, Vol. 15, No. 11, 796–798, Nov. 2005, https://doi.org/10.1109/LMWC.2005.859011.
2. Gao, Y.-Q., W. Shen, L. Wu, and X.-W. Sun, "Compact microstrip BPF with high selectivity using extended tapped lines," *Progress In Electromagnetics Research Letters*, Vol. 80, 39–46, 2018.
3. Huang, L., M. Li, P.-J. Zhang, K. Duan, and Y. Song, "A novel miniaturized UWB bandpass filter basing on E-shaped defected microstrip structure," *Progress In Electromagnetics Research Letters*, Vol. 93, 49–57, 2020.
4. Yechou, L., A. Tribak, M. Kacim, J. Zbitou, and A. M. Sanchez, "A novel wideband bandpass filter using coupled lines and T-shaped transmission lines with wide stopband on low cost substrate," *Progress In Electromagnetics Research C*, Vol. 67, 143–152, 2016.
5. Xiang, K.-R. and F.-C. Chen, "High selective and wide-stopband bandpass filter using simple uniform impedance resonators," *Progress In Electromagnetics Research Letters*, Vol. 80, 135–141, 2018.
6. Wang, Q., C. Shi, X. Xia, Z. Wang, and Y. Huang, "A compact ultra-wideband bandpass filter with sharp roll-off based on CPW-to-microstrip coupling structure," *Progress In Electromagnetics Research Letters*, Vol. 69, 127–132, 2017.
7. Garcia-Garcia, J., J. Bonache, and F. Martin, "Application of electromagnetic band gaps to the design of ultra-wide bandpass filters with good out-of-band performance," *IEEE Trans. Microw. Theory Techn.*, Vol. 54, No. 12, 4136–4140, Dec. 2006, https://doi.org/10.1109/TMTT.2006.886155.
8. Li, R. and L. Zhu, "Compact UWB bandpass filter using stub-loaded multiple-mode resonator," *IEEE Microw. Wireless Compon. Lett.*, Vol. 17, No. 1, 40–42, Jan. 2007, https://doi.org/10.1109/LMWC.2006.887251.

9. Wong, S. W. and L. Zhu, "EBG-embedded multiple-mode resonator for UWB bandpass filter with improved upper-stopband performance," *IEEE Microw. Wireless Compon. Lett.*, Vol. 17, No. 6, 421–423, Jun. 2007, https://doi.org/10.1109/LMWC.2007.897788.
10. Wong, S. W. and L. Zhu, "Quadruple-mode UWB bandpass filter with improved out-of-band rejection," *IEEE Microw. Wireless Compon. Lett.*, Vol. 19, No. 3, 152–154, Mar. 2009, https://doi.org/10.1109/LMWC.2009.2013735.
11. Jadhav, J. B. and P. J. Deore, "A compact planar ultra-wideband bandpass filter with multiple resonant and defected ground structure," *AEU — International Journal of Electronics and Communications*, Vol. 81, 31–36, 2017, ISSN 1434-8411, https://doi.org/10.1016/j.aeue.2017.07.003.
12. Mira, F., et al., "Design of ultra-wideband substrate integrated waveguide (SIW) filters in zigzag topology," *IEEE Microw. Wireless Compon. Lett.*, Vol. 19, No. 5, 281–283, May 2009, https://doi.org/10.1109/LMWC.2009.2017589.
13. Chen, R. S., et al., "Wideband bandpass filter using U-slotted substrate integrated waveguide (SIW) cavities," *IEEE Microw. Wireless Compon. Lett.*, Vol. 25, No. 1, 1–3, Jan. 2015, https://doi.org/10.1109/LMWC.2014.2363291.
14. Huang, L., et al., "Compact and high-performance UWB bandpass filter based on HMSIW," *Electron. Lett.*, Vol. 56, No. 22, 1181–1184, Oct. 2020, https://doi.org/10.1049/el.2020.1761.
15. Shang, Z., et al., "Design of a superconducting ultra-wideband (UWB) bandpass filter with sharp rejection skirts and miniaturized size," *IEEE Microw. Wireless Compon. Lett.*, Vol. 23, No. 2, 72–74, Feb. 2013, https://doi.org/10.1109/LMWC.2013.2239633.
16. Luo, X., et al., "Wideband bandpass filter with wide stopband using loaded BCMC Stub and short-stub," *IEEE Microw. Wireless Compon. Lett.*, Vol. 21, No. 7, 353–355, Jul. 2011, https://doi.org/10.1109/LMWC.2011.2157232.
17. Shang, Z., et al., "Design of a superconducting ultra-wideband (UWB) bandpass filter with sharp rejection skirts and miniaturized size," *IEEE Microw. Wireless Compon. Lett.*, Vol. 23, No. 2, 72–74, Feb. 2013, https://doi.org/10.1109/LMWC.2013.2239633.
18. Zhang, D., et al., "A compact wideband filter based on spoof surface plasmon polaritons with a wide upper rejection band," *IEEE Photonic Techn. Lett.*, Vol. 32, No. 24, 1511–1514, Dec. 2020, https://doi.org/10.1109/LPT.2020.3029290.
19. Liang, C. H. and C. Y. Chang, "Compact wideband bandpass filters using stepped-impedance resonators and interdigital coupling structures," *IEEE Microw. Wireless Compon. Lett.*, Vol. 19, No. 9, 551–553, Sep. 2009, https://doi.org/10.1109/LMWC.2009.2027060.
20. Chu, Q. X. and X. K. Tian, "Design of UWB bandpass filter using stepped-impedance stub-loaded resonator," *IEEE Microw. Wireless Compon. Lett.*, Vol. 20, No. 9, 501–503, Sep. 2010, https://doi.org/10.1109/LMWC.2010.2053024.
21. Chu, Q. X., X. H. Wu, and X. K. Tian, "Novel UWB bandpass filter using stub-loaded multiple-mode resonator" *IEEE Microw. Wireless Compon. Lett.*, Vol. 21, No. 8, 403–405, Aug. 2011, https://doi.org/10.1109/LMWC.2011.2160526.
22. Taibi, et al., "A novel design method for compact UWB bandpass filters," *IEEE Microw. Wireless Compon. Lett.*, Vol. 25, No. 1, 4–6, Jan. 2015, https://doi.org/10.1109/LMWC.2014.2363016.
23. La, D.-S., X. Guan, M.-Y. Wang, and R.-Q. Mi, "Compact wideband bandpass filter based on coupled line stub with high selectivity," *AEU — International Journal of Electronics and Communications*, Vol. 138, 153872, 2021, ISSN 1434-8411, https://doi.org/10.1016/j.aeue.2021.153872.
24. Iqubal, A. and P. Abdulla, "Bandpass filter based on asymmetric funnel shaped resonators with ultra wide upper stopband characteristics," *AEU — International Journal of Electronics and Communications*, Vol. 116, 153062, 2020, ISSN 1434-8411, https://doi.org/10.1016/j.aeue.2020.153062.
25. Ghazali, A. N., M. Sazid, and S. Pal, "Multiple passband transmission zeros embedded compact UWB filter based on microstrip/CPW transition," *AEU — International Journal of Electronics and Communications*, Vol. 129, 153549, 2021, ISSN 1434-8411, https://doi.org/10.1016/j.aeue.2020.153549.
26. Lan, S. W., et al., "Design of a compact ultra-wideband bandpass filter with an extremely broad stopband region," *IEEE Microw. Wireless Compon. Lett.*, Vol. 26, No. 6, 392–394, Jun. 2016,

https://doi.org/10.1109/LMWC.2016.2558039.

27. Zhou, C. X., et al., "Design of a compact UWB filter with high selectivity and superwide stopband," *IEEE Microw. Wireless Compon. Lett.*, Vol. 27, No. 7, 636–638, Jun. 2017, https://doi.org/10.1109/LMWC.2017.2711509.
28. Zhou, J., Y. Rao, D. Yang, H. J. Qian, and X. Luo, "Compact wideband BPF with wide stopband using substrate integrated defected ground structure," *IEEE Microw. Wireless Compon. Lett.*, Vol. 31, No. 4, 353–356, Apr. 2021, https://doi.org/10.1109/LMWC.2021.3053756.
29. Xu, J., "Compact quasi-elliptic response wideband bandpass filter with four transmission zeros," *IEEE Microw. Wireless Compon. Lett.*, Vol. 25, No. 3, 169–171, Mar. 2015, https://doi.org/10.1109/LMWC.2015.2390571.
30. Killamsetty, V. K. and B. Mukherjee, "Compact wideband bandpass filter for TETRA band applications," *IEEE Microw. Wireless Compon. Lett.*, Vol. 27, No. 7, 630–632, Jul. 2017, https://doi.org/10.1109/LMWC.2017.2711515.
31. Yang, Q., M. Shu, C. Guo, J. Li, and A. Zhang, "High selectivity wideband bandpass filter based on stepped impedance open stubs loaded ring resonator," *AEU — International Journal of Electronics and Communications*, Vol. 126, 153408, 2020, ISSN 1434-8411, https://doi.org/10.1016/j.aeue.2020.153408.